The Function of Amino Acid Residues Contacting the Nicotinamide Ring of NADPH in Dihydrofolate Reductase from *Escherichia coli*†

Joseph A. Adams,‡ Carol A. Fierke,§ and S. J. Benkovic*,‡

Department of Biochemistry, Duke University Medical Center, Durham, North Carolina 27710, and Department of Chemistry, The Pennsylvania State University, 152 Davey Laboratory, University Park, Pennsylvania 16802

Received June 12, 1991; Revised Manuscript Received August 29, 1991

ABSTRACT: The importance of three amino acid residues contacting the nicotinamide ring of NADPH in *Escherichia coli* dihydrofolate reductase has been defined using site-directed mutagenesis and detailed steady-state and pre-steady-state kinetic experiments. Replacement of Tyr-100 with either glycine or isoleucine (Y100G or Y100I) disrupts an aromatic–aromatic interaction between the phenolic side chain and the nicotinamide ring. Both mutations remove the differential binding of the oxidized and reduced coenzymes implicating Tyr-100 as a major determinant for coenzyme specificity. Replacement of Ser-49 for alanine (S49A), designed to either displace or reduce the polarizability of a bound water molecule contacting the N1 of the nicotinamide ring, affects only the rate of release of $NADP^+$. Replacement of Ile-14 with alanine (I14A), designed to alter both a weakly polar and a hydrogen bonding interaction with the periphery of the nicotinamide ring, affects only the binding of NADPH. Y100I, Y100G, and I14A all increase the activation barrier for the chemical step by approximately 2 kcal/mol. The lack of an effect for S49A suggests that water structure is not important for stabilizing the hydride transfer transition state. In addition, the nominal effects observed for these mutations disfavor the hypothesis that neighboring amino acid residues participate in the stabilization of the reaction transition state through polar or weakly polar contacts.

Dihydrofolate reductase (DHFR)[1] (5,6,7,8-tetrahydrofolate:$NADP^+$ oxidoreductase) catalyzes the reduction of dihydrofolate (H_2F) to tetrahydrofolate (H_4F) by stereospecific hydride transfer from the nicotinamide of NADPH to C6 of the pterin ring of H_2F. Due to the critical role of derivatized forms of H_4F for purine and thymidylate biosynthesis, the enzyme has been targeted for drug chemotherapy. For example, methotrexate [MTX] is a tight binding inhibitor that halts DNA synthesis in proliferating cancer cells by nucleotide deprivation. X-ray crystallographic data on the binary MTX (Matthews et al., 1977) and ternary $NADP^+$/folate (Bystroff et al., 1990) complexes reveal key interactions made at both the coenzyme and substrate binding sites. Dihydrofolate occupies a deep cavity making a large number of conserved hydrophobic contacts (e.g., Leu-54, Phe-31, Ile-50, and Leu-28), Asp-27, the only ionizable group in the active-site interior, delivers a proton to N5 of the pteridine ring. The coenzyme binds in an extended conformation with the nicotinamide ring closely positioned to the pterin ring. A number of hydrophobic (e.g., Tyr-100, Ile-14) and hydrogen bonding (e.g., Ser-49) interactions are made between the protein and the nicotinamide ring of NADPH.

DHFR catalyzes a very rapid and highly favorable hydride transfer reaction. Due to a hybridization change in the nicotinamide ring, a mechanism whereby the reduction step is facilitated by peripheral residues interacting with the developing pyridinium cation is possible. The enzyme may also achieve high efficiency by orienting reactant ground states so that they can make close contact. To probe for subtle mechanisms for stabilization of the nicotinamide ground and transition states through either polar, weakly polar, or steric contacts, three conserved residues (Tyr-100, Ser-49, and Ile-14) surrounding the ring were replaced using site-directed mutagenesis. The mutant proteins' abilities to bind ligands and to catalyze H_2F reduction were then assessed using binding, steady-state, and pre-steady-state kinetic techniques. The effects of specific mutations are discussed in light of the complete kinetic mechanism of wild-type DHFR from *Escherichia coli* (Fierke et al., 1987).

Materials and Methods

Mutant Enzymes. S49A was constructed from plasmid pLLc1-1, which contains an oligonucleotide cassette encompassing the coding region for the α-helix of *E. coli* DHFR (Li & Benkovic, 1991). The above was digested with the restriction endonucleases *Nar*I and *Eag*I. The large DNA fragment was purified by an agarose gel/DEAE membrane procedure as previously described (Winberg & Hammarskjold, 1980). The mutagenic double-stranded DNA (50 pmol) shown below (mutation in the box), which contains the sticky ends

```
5'CGC CAT ACC TGG GAA |GAT| ATC-3'
   G GTA TGG ACC CTT |CTA| TAG CCG G
```

compatible with those generated by *Nar*I and *Eag*I digestion of pLLc1-1, was ligated to the purified, linearized DNA (1 pmol) by T4 DNA ligase (Legerski & Robberson, 1985). The circular DNA was then transformed into *E. coli* strain w71-18 by the method of Hanahan (1983). Cells containing the transformed plasmid were segregated on LB/agar plates containing 25 μg/mL chloramphenicol and 10 μg/mL tri-

† This work was supported by NIH Grant GM24129.

* Author to whom correspondence should be addressed.
‡ The Pennsylvania State University.
§ Duke University Medical Center.

[1] DAM, 2,4-diamino-6,7-dimethylpteridine; DHFR, *E. coli* dihydrofolate reductase; H_2F or D or DHF, 7,8-dihydrofolate; H_4F or T, 5,6,7,8-tetrahydrofolate; I14A, isoleucine-14 → alanine DHFR mutant; MTX, methotrexate; NADPD, [(4′*R*)-^{2}H]NADPH; NADPH or NH, nicotinamide adenine dinucleotide phosphate reduced; $NADP^+$ or N, nicotinamide adenine dinucleotide phosphate; S49A, serine-49 → alanine DHFR mutant; Y100G, tyrosine-100 → glycine DHFR mutant; Y100I, tyrosine-100 → isoleucine DHFR mutant.

0006-2960/91/0430-11046$02.50/0 © 1991 American Chemical Society

methoprim. Several colonies were selected and sequenced using [γ-^{35}S]dATPγS (Sanger et al., 1977) in the region of the cassette (approximately 40 bases before and after the cassette). The mutant plasmid was then transformed into w71-18.

Y100I, Y100G, and I14A were obtained by primer extension of oligonucleotides (Zoller & Smith, 1982; Smith, 1985). The template was partially single-stranded DNA in which a 1-kb fragment containing the DHFR (fol) gene (Smith & Calvo, 1980) was inserted in the *Bam*HI site of a 4.4-kb pBR322 derivative plasmid lacking the *Eco*RI site (Chen et al., 1987). Mutant DNA was identified by either colony hybridization (Wallace et al., 1981) or restriction enzyme analysis since the mutagenic oligonucleotides introduced new restriction sites as shown below (I14A inserts an additional

```
I14A :  TA  GAT GGC  GTT  GC C  GGC  ATT G
Y1001 :  GGC GGC  GG A  CGC  GTT AT T  GAA CAG
Y100G :  GGC GGC  GG A  CGC  GTT GG T  GAA CAG
```

*Nae*I site and Y100I and Y100G insert a unique *Mlu*I site; sites are underlined and mutations are enclosed in boxes). The entire DHFR gene of the mutant DNA was sequenced according to Sanger et al. (1977). The correct mutant DNA was then transformed into HB101.

S49A was purified with the aid of a MTX affinity resin (Baccanari et al., 1975). However, the protein was eluted with a high salt buffer (1 M KCl) rather than 1 mM folic acid because of the mutant's poor binding to MTX at high salt concentration. Y100G could not be purified by the affinity resin owing to its weak binding properties so the affinity resin was replaced with a Sephadex G-75 column. Crude enzyme extracts were concentrated by AMICON filtration (YM-10 filter) and then applied to a 2.5 × 50 cm column equilibrated with 50 mM Tris/1 mM EDTA/1 mM DTE, pH 7.2. All fractions containing activity were pooled and then subjected to anion-exchange chromatography as previously described (Baccanari et al., 1975). I14A and Y100I were purified by MTX affinity and anion-exchange chromatography (Baccanari et al., 1975). Homogeneity of the protein samples was determined by polyacrylamide electrophoresis. The absence of ligand contamination was ascertained by $A^{280}/A^{260} = 1.7$–1.9 (for nucleotides) and $A^{350} \simeq 0$ (for folate).

Materials. 7,8-Dihydrofolate was prepared by the dithionite reduction of folic acid (Blakely, 1960) and (6*S*)-tetrahydrofolate was prepared from H_2F by enzymatic conversion with DHFR (Matthews & Huennekens, 1960). Purification of H_4F was achieved on a DE-54 resin with a linear triethylammonium bicarbonate gradient (Curthoys et al., 1972). NADPH, $NADP^+$, MTX, and folic acid were purchased from Sigma. 2,4-Diamino-6,7-dimethylpteridine (DAM) was purchased from ICN Pharmaceuticals. [(4′*R*)-^{2}H]NADPH (NADPD) was prepared using *Leuconostoc mesenteroides* alcohol dehydrogenase purchased from Research Plus, Inc. and was purified by the method of Viola et al. (1979). Excess NaCl was removed from the purified NADPD by a Bio-Gel P-2 desalting column (Howell et al., 1987).

All ligand concentrations were determined spectrophotometrically by using the following extinction coefficients: H_4F, 28 000 M^{-1} at 297 nm, pH 7.5 (Kallen & Jencks, 1966); H_2F, 28 000 M^{-1} at 282 nm, pH 7.4 (Dawson et al., 1969); folic acid, 27 600 M^{-1} at 282 nm, pH 7.0 (Rabinowitz, 1960); MTX, 22 100 M^{-1} at 302 nm in 0.1 N KOH (Seeger et al., 1949); NADPH, 6200 M^{-1} at 339 nm, pH 7.0; $NADP^+$, 18 000 M^{-1} at 259 nm, pH 7.0 (P-L Biochemicals, 1961). The concentrations of H_2F and NADPH were also checked by turnover with DHFR. Endonucleases were purchased from New England Biolabs. T4 DNA ligase was purchased from IBI. All kinetic measurements were obtained at 25 °C in a buffer which contained 50 mM 2-(*N*-morpholino)ethanesulfonic acid, 25 mM tris(hydroxymethyl)aminomethane, 25 mM ethanolamine, and 100 mM sodium chloride (MTEN buffer). The buffers were purged with argon and contained 1 mM dithiothreitol when H_4F was used. All kinetic experiments were done at pH 7 unless otherwise noted.

Steady-State Kinetics. Initial velocities for the enzyme reactions were measured by using a Cary 219 UV–visible spectrophotometer. The molar absorbance change was 11 800 M^{-1} (Stone & Morrison, 1982). All pH-dependent steady-state data were fit to

$$C = C_{max}[H]/([H] + K_a) \quad (1)$$

where C and C_{max} are, respectively, the pH-dependent and pH-independent values of either V or V/K and K_a is the acid dissociation constant associated with these parameters. The enzyme was preequilibrated with NADPH before the addition of H_2F. The inhibition constant of DAM, $K_{i,obs}$, was measured for both mutants by plotting $1/v$ vs [DAM] (Segel, 1975; Stone & Morrison, 1982). $K_{i,app}$ was then obtained from $K_{i,obs}$ by the equation

$$K_{i,app} = K_{i,obs}/(1 + [H_2F]/K_M) \quad (2)$$

The values of $K_{i,app}$ were then fit to the equation

$$K_{i,app} = K_I(1 + [H]/K_b)(1 + K_a/[H]) \quad (3)$$

where K_I is the pH-independent dissociation constant of DAM and K_a and K_b are the acid dissociation constants of the free enzyme and DAM, respectively.

Stopped-Flow Kinetics. Transient binding and pre-steady-state kinetics for Y100I, Y100G, and I14A were performed on a stopped-flow apparatus designed and built in the laboratory of Dr. Kenneth A. Johnson (1986). The instrument has a dead time of 1.6 ms and a 2-mm sample cell and can be used in either a transmittance or fluorescence mode. Interference filters (Corion Corp.) were used for emission output, and a monochromator was used for excitation input. Typically, ligand binding experiments were monitored by using a selected wavelength of 290 nm and an output filter of 340 nm. To measure coenzyme fluorescence, an output filter of 450 nm was used. Absorbance was measured at 340 nm by conversion of transmittance data. Following a trigger impulse, data were collected by a computer over a selected time range. In most cases, an average of 6–10 traces was taken at a given set of conditions for data analysis. Kinetic data were fit using a nonlinear least-squares computer program that analyzed the transients as a single- or double-exponential rate constant or a single-exponential rate constant followed by a linear rate (Dyson & Isenberg, 1971; Johnson, 1986). Pre-steady-state data were transferred to a Vax microcomputer and fit to more complicated mechanisms using the kinetic simulation program KINSIM (Barshop et al., 1983).

All rapid kinetic experiments for S49A were performed on a stopped-flow apparatus puchased from Applied Photophysics.

Fluorescence Titrations. The thermodynamic binding of ligands (K_d) was measured by following the quenching of the intrinsic enzyme fluorescence at 340 nm upon excitation at 290 nm as a function of added ligand on an SLM 8000 spectrofluorometer. In separate control experiments, a known quantity of tryptophan was titrated to correct for inner filter absorbance effects of the ligand. Typically, the enzyme

Table I: Steady-State Kinetic Parameters for Mutant and Wild-Type DHFRs[a]

	mutants				
	I14A	Y100I	Y100G	S49A	WT[b]
k_{cat} (s^{-1})	15 ± 1.7	3.8 ± 0.26	2.9 ± 0.15	9.7 ± 2.6	12
$pK_a(k_{cat})$	7.5 ± 0.1	7.2 ± 0.1	8.2 ± 0.1	8.3 ± 0.2	8.4
k_{cat}/K_M^{NH} ($\times 10^4$ M^{-1} s^{-1})	280 ± 30	52 ± 8	71 ± 59	210 ± 60	210
$pK_a(k_{cat}/K_M^{NH})$	7.4 ± 0.1	7.2 ± 0.1	8.1 ± 0.1	8.3 ± 0.2	

[a] k_{cat} and k_{cat}/K_M^{NH} are pH-independent values, 25 °C. [b] k_{cat} and $pK_a(k_{cat})$ for wild-type DHFR were measured at 100 μM NADPH and varying H_2F. k_{cat}/K_M was measured with 10 μM H_2F and 1–100 μM NADPH at pH 7 (Fierke et al., 1987).

Table II: Thermodynamic Dissociation Constants for Ligands to Mutant and Wild-Type DHFRs at pH 7.0, 25 °C

	K_d (μM)				
ligand	I14A	Y100I	Y100G	S49A	WT[a]
NADPH	1.4 ± 0.1	6.5 ± 0.15	7.7 ± 0.46	0.23 ± 0.04	0.33
$NADP^+$	25 ± 1.3	5.7 ± 0.27	22 ± 2.5	7.3 ± 1.1	24
H_2F	0.22 ± 0.07	0.12 ± 0.01	0.81 ± 0.09	0.21 ± 0.04	0.22

[a] Wild-type values were measured at pH 6 (Fierke et al., 1987).

concentration was either at or slightly less than the K_d of the ligand. The data were fit to the equation

$$F = F_E - C(F_E - F_{EL})/2E_T \quad (4)$$

where

$$C = E_T + L_T + K_d - [(E_T + L_T + K_d)^2 - 4(E_T)(L_T)]^{1/2}$$

In this equation, E_T and L_T are the total enzyme and ligand concentrations, respectively, F_E is the initial fluorescence, and F_{EL} is the final fluorescence. The data were fit with a nonlinear least-squares program previously described (Taira & Benkovic, 1988).

Results

Steady-State Kinetics. The steady-state kinetic parameters, k_{cat} and k_{cat}/K_M, for the reaction of the mutants with varying amounts of NADPH and fixed H_2F (50 μM) are presented in Table I. The latter substrate was saturating since doubling its concentration had no effect on the reaction rate. There was no evidence for two K_Ms for NADPH binding to two differing forms of the enzyme, E–H_2F and E–H_4F. The observed deuterium isotope effects on k_{cat} at high pH using NADPD are 2.7 ± 0.1 for Y100I (pH 9), 3.0 ± 0.1 for Y100G and I14A (pH 10), and 3.0 ± 0.3 for S49A (pH 10). At low pH, the isotope effects are 1.6 ± 0.2 for Y100I (pH 6), 1.7 ± 0.2 for Y100G (pH 6), 1.5 ± 0.1 for I14A (pH 5.7), and 1.0 ± 0.2 for S49A (pH 6). The rates of k_{cat} in the reverse direction (i.e., conversion of $NADP^+$ and H_4F to NADPH and H_2F) were measured by mixing 1–1.5 mM $NADP^+$ and 20–250 μM H_4F with the mutant at pH 9. The observed rates for these reactions were unaffected by increasing the pH to 10. The pH-independent k_{cat} values were determined to be 0.025 ± 0.002 s^{-1}, 0.21 ± 0.03 s^{-1}, and 0.064 ± 0.003 s^{-1} for Y100G, Y100I, and I14A, respectively.

Thermodynamic Binding of Ligands. The thermodynamic binding of ligands (K_d) to mutant DHFRs was analyzed by following the quenching of the intrinsic enzyme fluorescence (excitation λ = 290 nm, emission λ = 340 nm) upon ligand titration (Birdsall et al., 1980; Stone & Morrison, 1984). Table II shows the K_ds of various ligands binding to both mutant and wild-type enzymes. Overall, the effects appear localized at the nicotinamide site. The following discussion will illustrate some of the pitfalls in using K_d measurements as the sole determinants for ligand binding to these mutants.

Scheme I

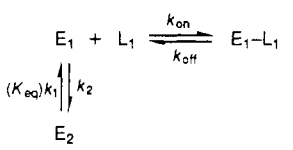

Table III: Association and Dissociation Rate Constants of Ligands to Mutant and Wild-Type DHFRs at pH 7.0, 25 °C

	k_{on} (μM^{-1} s^{-1})			k_{off} (s^{-1})		
ligand	I14A	S49A	WT[a]	I14A	S49A	WT[a]
NADPH	30 ± 5	22 ± 2	20	85 ± 15	5 ± 4	3.5
$NADP^+$		5.1 ± 3	13		290 ± 50	300
H_2F	3.5 ± 0.8	46 ± 6	40	23 ± 4	38 ± 6	40
H_4F	4.0 ± 0.6		25	6 ± 5		<1

[a] Fierke et al. (1987).

Kinetic Binding of Ligands. The transient binding of ligands can be monitored by following the time-dependent quenching of the intrinsic enzyme fluorescence upon stopped-flow mixing of the ligand with enzyme (Dunn et al., 1978; Dunn & King, 1980; Cayley et al., 1981). Cayley et al. (1981) have concluded that the enzyme exists in two slowly interconverting forms, E_1 and E_2, of which only one binds ligands, E_1. This mechanism is illustrated in Scheme I and gives rise to a raid ligand-dependent phase and a slower ligand-independent phase upon mixing.

For pseudo-first-order reaction conditions ([L] ≫ [E]), the observed rate constant, (k_{obs}, for binding L_1 to E_1 (the ligand-dependent phase) can be approximated by $k_{obs} = k_{on}$ [L] + k_{off} where k_{on} and k_{off} are the association and dissociation rate constants, respectively. A plot of k_{obs} vs [L] yields k_{on} from the slope and k_{off} from the intercept. The association and dissociation rate constants for several ligands to the mutants are listed in Table III. The rate constant for enzyme interconversion, k_1, is determined from the slow-phase rate while the equilibrium constant, $K_{eq} = k_1/k_2$, is calculated from the ratio of the amplitudes of the two phases. For the wild type and the mutants the following kinetic constants were determined: k_1 = 0.03 s^{-1} (WT), 0.065 ± 0.04 s^{-1} (I14A), and 0.047 ± 0.004 (S49A); K_{eq} = 1 (WT), 0.89 ± 0.09 (I14A), and 2.3 ± 0.5 (S49A). For S49A, a phase of 30 s^{-1} was observed in addition to the slow protein isomerization upon the binding of $NADP^+$. This phase did not increase in rate or amplitude between 16 and 500 μM $NADP^+$ (data not shown) and, thus, could not be ascribed to a ligand association step.

Attempts at measuring association and dissociation rate constants for Y100I and Y100G by a relaxation method failed because of low amplitudes for the fast phase. However, both mutants showed measurable ligand-independent phases with a rate constant similar to k_1 for wild-type DHFR and I14A (data not shown). Therefore, the ratio of the amplitude of fast phase to slow phase is much less than one, and since measurement of the enzyme interconversion is dependent on the tryptophan quenching associated with ligand binding, this result indicates that K_{eq} for both Y100I and Y100G is also much less than one so that the predominant, unliganded enzyme species is E_2. For this reason we chose an alternative route for measuring the equilibrium of the native enzyme conformers (see next section).

Dissociation Rate Constants for Ligands. The dissociation rate constants of ligands from DHFR can be measured independently by using a competition method (Dunn et al., 1978). In this technique the enzyme–ligand complex ($E–L_1$)

Table IV: Dissociation Rate Constants of Ligands from Mutant and Wild-Type DHFRs at pH 7.0, 25 °C

ligand	enzyme species[a]	k_{off} (s^{-1}) I14A	S49A	Y100I	Y100G	WT[b]
NADPH	E-NADPH	80 ± 5	5.6 ± 0.5	26 ± 3	2.8 ± 0.6	3.6
	E-NH-H_4F			100 ± 15		85
$NADP^+$	E-$NADP^+$	175 ± 20	23 ± 3[c]	6 ± 0.7	5.2 ± 0.4	290
	E-N-H_4F	210 ± 40	23 ± 3[c]	5 ± 0.4	3.3 ± 0.5	200
H_2F	E-H_2F	22 ± 4	23 ± 1	7 ± 1	18 ± 2	22
H_4F	E-H_4F	8.3 ± 1	2.9 ± 0.1	1.4 ± 0.1	15 ± 1	1.4
	E-N-H_4F	8.8 ± 0.8	4.6 ± 0.1	14 ± 1	21 ± 2	2.4
	E-NH-H_4F	30 ± 3	20 ± 1	14 ± 2	23 ± 2	12

[a] MTX was used to compete for complexes with H_2F and H_4F while $NADP^+$ was used to compete for complexes with NADPH and $NADP^+$ for NADPH. [b] Measured at pH 6 (Fierke et al., 1987). [c] The liberation of $NADP^+$ was monitored by fluorescence energy transfer.

Scheme II

$$E\text{–}L_1 \underset{k_1}{\overset{k_{-1}}{\rightleftharpoons}} E + L_1$$

$$E + L_2 \underset{k_{-2}}{\overset{k_2}{\rightleftharpoons}} E\text{–}L_2$$

is preequilibrated before a large excess of a competing ligand (L_2) is rapidly mixed in a stopped-flow apparatus. If there is a sufficient difference in the fluorescence properties of E–L_1 and E–L_2 then an exponential rate constant is observed. This process is described in Scheme II.

When $k_1[L_1] \ll k_2[L_2] \gg k_{-1}$, the observed rate constant, k_{obs}, is equal to the dissociation rate constant for L_1, k_{-1}. The off rates of a number of ligands from binary and ternary complexes of the mutants were determined by using this technique. These results along with those of wild-type DHFR are shown in Table IV. Although the dissociation rate constants of ligands from Y100I and Y100G could not be directly measured in a relaxation experiment, the off rates could be measured in a competition experiment since this technique relies on the net difference in protein fluorescence between two ligand-bound complexes and is independent of the ratio of E_1 and E_2.

Pre-Steady-State Kinetics. The hydride transfer rate constant, k_{hyd}, for wild-type DHFR has been isolated by using pre-steady-state fluorescence energy transfer experiments (Fierke et al., 1987). In this technique, the protein emission at 340 nm excites the nicotinamide portion of NADPH, which in turn emits at 450 nm. Since the oxidized nicotinamide of $NADP^+$ displays no emission in this spectral region and the transfer process is highly distance-dependent (Stryer & Haughland, 1967), the consumption of NADPH as well as any protein or coenzyme conformational changes that alter the fluorophore environment in the first turnover can be monitored.

The observed k_{hyd}^{app} for mutants was determined by using stopped-flow fluorescence energy transfer. A typical pre-steady-state transient for I14A at pH 6.8 is shown in Figure 1. In this experiment, 11 μM enzyme and 45 μM H_2F were preequilibrated before 100 μM NADPH or NADPD was rapidly mixed. Both transients could be fit to a single-exponential decay followed by a linear phase (k_L). For NADPH, a burst rate constant, k_{hyd}^{app}, of 33 ± 3 s^{-1} and a linear rate constant, k_L, of 11.9 s^{-1} were observed. This burst was confirmed to be the hydride transfer step since repeating the experiment with NADPD gave a deuterium kinetic isotope effect ($^Dk_{hyd}^{app}$) of 3.0 ± 0.2 and ^Dk_L of 1.6. Similar kinetic behavior was observed for the other mutants. These data are listed in Table V. All mutants showed deuterium isotope effects on the burst phase of approximately 3. Except in the case of I14A, the mutants were prequilibrated with the coenzyme rather than H_2F. I14A required preequilibration with

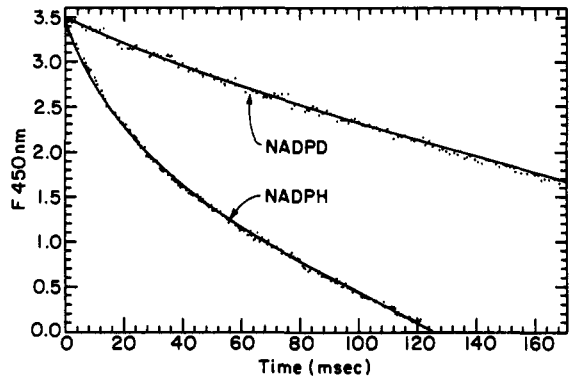

FIGURE 1: Measurment of the pre-steady-state burst for I14A by stopped-flow fluorescence energy transfer. DHFR is preincubated with H_2F, and the reaction is initiated with either NADPH or NADPD. The solid line is simulated by KINSIM (Barshop et al., 1983) using Scheme III and the rate constants discussed in the text. Final conditions: 11 μM I14A, 100 μM NADPH(D), 45 μM H_2F, pH 6.8, 25 °C.

Table V: Values of Rate Constants for Hydride Transfer for the Various Mutants

mutant	k_{hyd}^{app}(s^{-1})	$^Dk_{hyd}^{app}$	k_L (s^{-1})	^Dk_L
I14A[a]	33 ± 3	3.0 ± 0.2	11.9	1.6
Y100I[b]	28 ± 2	2.8 ± 0.2		1.5
Y100G[c]	12 ± 1.2	2.8 ± 0.2		1.7
S49A[d]	120 ± 10	2.7 ± 0.3		1.0

[a] pH 6.8. [b] pH 5.8. [c] pH 6.5. [d] pH 7.0.

Scheme III

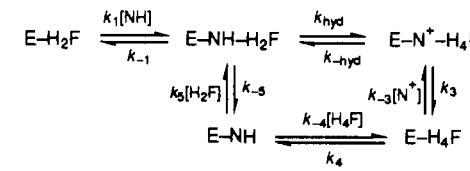

H_2F due to this ligand's reduced association rate constant (Table III).

For wild-type DHFR, k_{hyd}^{app} increases with decreasing pH until a pH-independent plateau is reached (Fierke et al., 1987). From these data a pK_a of 6.5 and a maximal hydride rate constant, k_{hyd}, of 950 s^{-1} for the protonated ternary complex were determined. The k_{hyd}^{app} values for the mutants were also pH-dependent. For I14A, Y100I, Y100G, and S49A, k_{hyd} = 48 ± 3, 35 ± 4, 15 ± 1, and 900 ± 150 s^{-1}, respectively, and pK_a(k_{hyd}) = 7.0 ± 0.1, 6.2 ± 0.2, 7.0 ± 0.1, and 6.4 ± 0.2, respectively. These values were determined either by direct fitting of the pre-steady-state transients to an exponential decay followed by a linear phase or by fitting to Scheme III with KINSIM (Barshop et al., 1983) as illustrated for I14A. For the latter mutant the rate constants for binding NADPH and H_2F (k_1, k_{-1}, k_5, and k_{-5}) were obtained from Table III. The

binding of H_2F was assumed to be unaffected by the presence of NADPH. The dissociation rate constants for $NADP^+$ (k_3) and H_4F (k_4) were measured directly (Table IV). (The binding of NADPH is included in k_4 since association is rapid and the equilibrium is favorable.) The wild-type values of 5 μM^{-1} s^{-1} and 2 μM^{-1} s^{-1} were used to set k_{-3} and k_{-4}, respectively (Fierke et al., 1987).

Since hydride transfer is solely rate-determining in the reverse steady-state reaction, the internal equilibrium, K_{int}, can now be determined from the maximum forward and reverse hydride rate: K_{int} = 750 (48 s^{-1}/0.064 s^{-1}) for I14A.

pH-Dependent Inhibition with DAM. Stone and Morrison (1984) have shown that the pK_a of Asp-27 in the E–NADPH complex can be determined by measuring the pH-dependent dissociation constant, K_i, of the classical, competitive inhibitor 2,4-diamino-6,7-dimethylpteridine (DAM). Plots of pK_i vs pH are bell-shaped with the lower pK_a reflecting the free acid dissociation of DAM (pK_a = 5.7) and the higher pK_a reflecting that of the carboxyl of Asp-27. The pH-dependent inhibition of the mutants with DAM gave pK_a's of 7.3 ± 0.19, 6.2 ± 0.07, and 7.1 ± 0.04 for Y100G, Y100I, and I14A, respectively.

Discussion

Although the source of the hydride and proton in the DHFR-catalyzed reduction of H_2F is clearly established, the ordering of these transfer processes is poorly understood. Although pre-protonation of N5 may facilitate hydride delivery by enhancing charge development on C6, there are a number of observations which challenge this mechanism. For instance, both UV difference (Poe et al., 1974; Maharaj et al., 1990) and NMR spectroscopy (Selinsky et al., 1990) have shown that the N5 of folic acid and H_2F is not protonated over a wide pH range in binary complexes. However, if the rate of hydride transfer is dependent on the concentration of a N5-protonated species then changes in the acidity of the reaction's proton donor, Asp-27, may be correlated to changes in the rate of hydride transfer. This would follow if the dominant effect of the mutation is only to alter the pK_a of Asp-27. Nevertheless, to date, there is no clear relationship between the pK_a values of folate-directed mutants and the hydride step (Benkovic et al., 1988). In addition, there is no obvious, complementary charge or polar contact near N5 that could sustain a pre-protonation mechanism. Since the free pK_a for N5 of H_2F is approximately 2.6 (Maharaj et al., 1990) and the pK_a of Asp-27 is 6.5 in all ligand-bound complexes, the concentration of protonated species is negligible. Thus, the possibility of concerted or late proton transfer must be considered.

At the NADPH site a very similar dilemma arises. During the reduction of H_2F, the hybridization of the nicotinamide ring must change to accommodate the lost hydride ion and the newly developed positive charge on N1 of the ring. Hence, a mechanism whereby the reduction step is stabilized electrostatically by peripheral residues may exist. Alternatively, the enzyme may achieve its high efficiency mainly through substrate/coenzyme proximity effects. In other words, DHFR may have evolved primarily to orient reactant ground states so that they can make close contact. This latter assertion is in accord with the structural observation that the nicotinamide binding site of many dehydrogenases is primarily a hydrophobic surface with few charged or polar residues (Birktoft & Banaszak, 1984). However, the X-ray structure of DHFR is better refined than that of most dehydrogenases and reveals a number of potential contacts that may be important in charge complementation.

To probe for subtle mechanisms for polar stabilization of the nicotinamide ring, three conserved residues surrounding

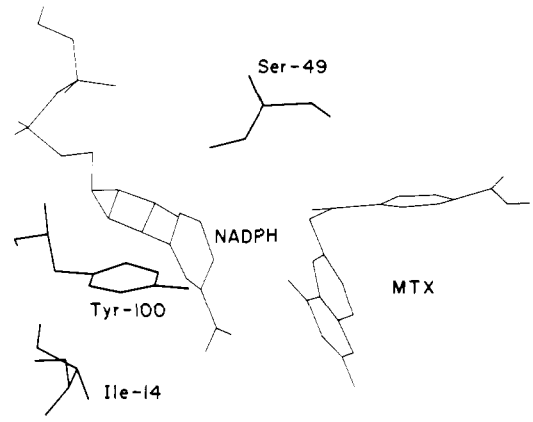

FIGURE 2: Nicotinamide binding site of *E. coli* DHFR. NADPH is modeled into the binary E–MTX complex (Benkovic et al., 1988).

the ring were replaced using site-directed mutagenesis. These residues and their proximity to the nicotinamide are illustrated in Figure 2. Tyr-100, which is a phenylalanine in all other known DHFRs, provides an aromatic–aromatic interaction with both the nicotinamide and the pterin rings. In addition, the polarizability of the phenolic side chain of Tyr-100 may contribute to stabilizing the positively charged nicotinamide in either the reaction transition state or product ground state complexes. Petsko and co-workers have cataloged the geometry of interactions of aromatic side chains (i.e., Phe, Tyr, and Trp) and amino groups (i.e., Lys, His, Arg, etc.) in 33 crystallographically refined protein structures (Burley & Petsko, 1986). The preferential arrangement of aromatic π electrons may offer large enthalpic contributions to structural stability and may also be important for catalysis. In addition to these potential contacts, recent crystallographic studies on the ternary E–$NADP^+$–fol complex of *E. coli* DHFR (Bystroff et al., 1990) have shown that the distance between the hydroxyl of Tyr-100 and the C4 of the nicotinamide ring is 2.8 Å. These authors have also modeled a theoretical transition state which incorporates a slightly puckered nicotinamide ring poised for hydride delivery. In this model, the hydroxyl–C4 distance is now partially relaxed to 3.0 Å. Thus, the function of the hydroxyl of Tyr-100 may be to promote the formation of the transition-state structure through the release of ground-state strain. Consequently, Tyr-100 was replaced with isoleucine (Y100I) and glycine (Y100G) to see whether the enzyme exploits either the polarizability of the phenolic group in order to stabilize the transition state or the steric bulk of the phenolic group to destabilize the reactant ground state.

The hydroxyl of Ser-49 interacts with the opposite face of the nicotinamide via a coordinated water molecule (the water molecule is not shown in Figure 2). Filman et al. (1982) have proposed that this conserved residue may be involved in the stabilization of the pyramidal nitrogen developing in the transition state. Under the presumption that the side chain of alanine is a conservative replacement for that of serine and offers no major disruptions in the protein fold, S49A at a minimum increases the mobility of the coordinated water molecule and alters its orientation, thus disrupting its interaction with the charged ring.

Finally, the carbonyl oxygen of Ile-14 makes close contact with the 2′-H and a H of the amide of the nicotinamide ring. Although the nicotinamide ring of the oxidized and reduced coenzymes is coplanar with the glycosidic bond and amide side chains, it has been asserted that a tetrahedral nitrogen forms in the transition state of formate dehydrogenase before collapse to an sp^2 center (Cook et al., 1981). On the basis of this analogy, Filman et al. (1982) have argued that a delocalized

Scheme IV

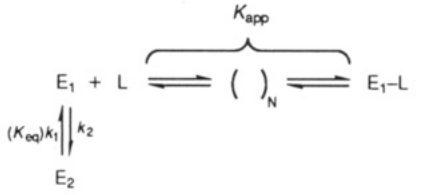

positive charge on the ring can be partially stabilized through a constellation of weakly polar interactions from several coplanar, carbonyl oxygens of which Ile-14 is one. It is compelling to note that three carbonyl oxygens are adjacent to C2, C4, and C6 of the nicotinamide of NADPH in *Lactobacillus casei* DHFR. These contacts are 0.2 Å shorter than ordinary van der Waals contacts and entertain the possibility of stabilizing partial carbonium ion character at the nicotinamide through weakly polar interactions. Similar contacts have been recently discovered in the NADP$^+$–folate ternary complex of *E. coli* DHFR (Bystroff et al., 1990). Consequently, isoleucine was replaced with alanine (I14A) in the hope of disturbing this interaction, presuming that the locus of the I14 carbonyl backbone would be influenced by side-chain interactions.

Ligand Binding. To prove that the association/dissociation of ligand with the mutant proteins can be analyzed by Scheme I (i.e., one-step association of ligand and E_1), three criteria were used: (1) the time-dependent fluorescent decay associated with binding must be ligand-dependent and purely monophasic, (2) the off rates measured by competition and relaxation methods must be equivalent, and (3) the individual rate constants for binding and conformer interconversion must scale to the overall dissociation constant, K_d, according to eq 5. For

$$K_d = k_{off}/k_{on}[1 + 1/K_{eq}] \quad (5)$$

wild-type enzyme there is evidence that ligand binding is actually more complicated than that in Scheme I in that the E_2 conformer may also bind ligands (Adams et al., 1990; Appleman et al., 1990), but since the affinity is decreased greatly this pathway contributes little to the overall kinetic pathway and can be ignored except at very high ligand concentrations.

For the binding of NADPH to I14A and S49A and H_2F to S49A, the above three criteria hold to within experimental error. However, all three fail for the binding of NADP$^+$ to S49A while for binding H_2F to I14A the third criterion is not met. Thus, the binding of these ligands is likely to be accompanied by a conformational change following formation of an initial collision complex. Further support for this interpretation has been observed in the case of NADP$^+$ binding to S49A. For this mutant and ligand combination a concentration-independent phase of 30 s^{-1} represents the sum of the forward and reverse rate constants for an enzyme–ligand isomerization. It is unlikely that this phase is due to ligand-bound conformer interconversion (i.e., E_1–NADP$^+$ → E_2–NADP$^+$) since the amplitude for such a transient would be negligible due to the high affinity of ligands for E_1 compared to E_2. Despite multiple forms of the binary enzyme–NADP$^+$ complex, the off rates for this ligand in various complexes are monophasic (Table III) and represent the net rate for the liberation of the oxidized coenzyme. The binding nature of NADP$^+$ to I14A could not be assessed by a relaxation method since its off rate is too large.

The three criteria could not be applied to the Y100 mutant protein since the association rate constants for ligands to Y100I and Y100G could not be measured directly owing to the low population of free E_1. However, the apparent dissociation rate constants for several ligands could be measured in a competition experiment (Table IV). Presuming a constant k_{on}, k_{off} can be used to compare the kinetic affinities of the various mutant proteins. The dissociation rate constant for NADP$^+$ is lowered approximately 10-fold for S49A, approximately 60-fold for Y100I and Y100G, and little changed for I14A. Because of the isomerization phase (30 s^{-1}) observed in the relaxation experiment for the S49A protein and the inability to determine k_{on} for the two latter mutants, these values may not represent the unimolecular dissociation rate constant for the oxidized coenzyme as outlined in Scheme I.

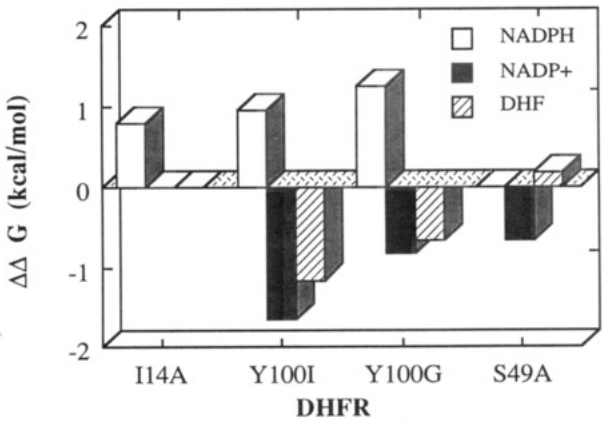

FIGURE 3: The affinity of NADPH, NADP$^+$, and H_2F (DHF) for the nicotinamide-directed mutants relative to wild-type DHFR. $\Delta\Delta G$ compares the free energy difference for the binding of these ligands on the basis of K_{app} (Scheme IV, eq 6). $\Delta\Delta G = \Delta G$(wild type) − ΔG(mutant).

An alternative approach was also taken in assessing the thermodynamic affinity of ligands in binary complexes. Under the assumption that E_1 is the preferred enzyme conformer for binding, the association of ligand and mutant can be described in Scheme IV. In this scheme, K_{app} denotes the net binding of ligand to the E_1 conformer with no assumption of intermediate complexes although they may indeed exist. (Additional forms of the enzyme–ligand complex are designated in the parentheses.) Thus, the thermodynamic binding to E_1 (K_{app}) is related to K_d and K_{eq} by the equation

$$K_{app} = K_d/(1 + 1/K_{eq}) \quad (6)$$

The binding affinities of several ligands and the mutants are compared to that of wild-type DHFR in Figure 3.

These results portray the differential effects of Tyr-100 replacement on the binding of NADPH and NADP$^+$. The mutants Y100I and Y100G tighten NADP$^+$ and loosen NADPH. In contrast, replacement of Ser-49 increases the binding affinity of NADP$^+$ to a value close to that for Y100I but has little effect on NADPH binding. The mutant S49A still binds NADPH 4–30-fold more tightly than NADP$^+$ on the basis of k_{off} and K_d. For I14A, only the binding of NADPH is decreased (4-fold). Thus, Tyr-100 is a unique switch that governs the binding specificity of *E. coli* DHFR for reduced and oxidized coenzyme.

In addition, the S49A, Y100I, and Y100G mutations affect the equilibrium constant between the two enzyme conformers, E_1 and E_2, which may hint at long-range structural effects. On the other hand, Bystroff et al. (1990) suggest that the cis/trans isomerization of the Gly-95–Gly-96 peptide bond is involved in E_1 to E_2 interconversion. Since Tyr-100 is close, it is conceivable that Y100I and Y100G substitutions may directly affect the equilibrium distribution of cis/trans isomers.

Overall Mechanism. A detailed kinetic mechanism for *E. coli* DHFR has been determined from steady-state and pre-steady-state absorbance and fluorescence spectroscopy that

predicts all the steady-state as well as full time course kinetics (Fierke et al., 1987). Several important features of this mechanism are (1) hydride transfer is rapid (950 s^{-1}) and highly favorable ($K_{int} \approx 1000$); (2) the initial, random binding of NADPH and H_2F becomes ordered under catalytic cycling owing to the faster release of $NADP^+$ compared to H_4F; (3) the dissociation of H_4F is fastest from the mixed ternary complex E–NADPH–H_4F (12 s^{-1} in the ternary vs 1.6 s^{-1} in the binary complexes; Table IV); and (4) the overall equilibrium favors product formation ($K_{ov} \approx 10^{11}$ M^{-1}), which is made up partly in the assymetric internal equilibrium ($K_{int} \approx 1500$ using a pH-independent number). In addition, the rapid proton exchange of Asp-27 ($pK_a = 6.5$) with solvent accounts for the equilibrium attenuation of hydride transfer at high pH (>7). Thus, the pH dependence of k_{cat} for H_2F reduction can be described by a change in the rate-limiting step from product release (12 s^{-1}) at low pH to hydride transfer at high pH.

All the mutants studied give rise to a full primary isotope effect at high pH using NADPD, indicating that hydride transfer controls k_{cat}. With the exception of S49A, partial isotope effects are observed for the mutants at low pH. Discrete observation of the chemical step by pre-steady-state fluorescence energy transfer and the product dissociation steps by competition clearly define kinetic mechanisms for Y100I, Y100G, and I14A that involve partial limitation of k_{cat} (low pH) by hydride transfer and product dissociation. For I14A, k_{cat} (14 s^{-1}; Table I) is controlled by the dissociation of H_4F (30 s^{-1}; Table IV) and hydride transfer (48 s^{-1}) while for Y100I and Y100G, k_{cat} (3.8 and 2.9 s^{-1}; Table I) is governed by hydride transfer (35 and 15 s^{-1}), H_4F (14 and 21 s^{-1}), and $NADP^+$ dissociation (6 and 5.2 s^{-1}). For S49A, the dissociation of H_4F and $NADP^+$ (20 and 23 s^{-1}; Table IV) share equally in the rate limitation of k_{cat} (9.7 s^{-1}; Table I).

The binding of NADPH to form the mixed ternary complex, E–NADPH–H_4F, accelerates the dissociation of H_4F in all mutants except Y100G by a factor of 3–10 (Table IV). This is consistent with the 6-fold increase found in the wild-type enzyme. For the wild-type and mutant enzymes except Y100I, $NADP^+$ does not markedly affect the release of H_4F. All mutants studied have little effect on the pK_a values of Asp-27 which are shifted less than 0.5 unit in the ternary complexes.

The marked attenuation of $NADP^+$ release (k_{off}) by Y100I and Y100G and, to a lesser extent, by S49A has a profound effect on the DHFR mechanism. The switch from rate-determining H_4F dissociation to $NADP^+$ release is highly unexpected. We conclude from this study that the functions of Tyr-100 and Ser-49 are to destabilize bound $NADP^+$, thereby promoting rapid product release. Introduction of smaller residues via mutagenesis may open the site for water facilitating nicotinamide binding which is not favored by the original hydrophobic pocket. It is not clear, however, without structural evidence why the effects of Tyr-100 replacement exceed that of Ser-49 or, more importantly, why the former substitutions are accompanied by a larger specificity change in the NADPH/$NADP^+$ pair. As expected, the effects in the folate site are smaller (Figure 3).

Comparison of Hydride Transfer Rates. DHFR employs amino acid residues of varying polarity at the active site. Hydrophobic contacts are made at the pterin and nicotinamide rings, and the hydrogen bonding and electrostatic contacts are primarily made at the tail regions of the coenzyme and substrate. Despite the nature of these interactions, the effects on the rates of hydride transfer are fairly equivalent with no individual residue contributing more than 2 kcal/mol to the transition-state stabilization (Figure 4). For instance, replacement of the distal arginine contacting the 2′-phosphate of NADPH gives a decrease in hydride similar to those of the nicotinamide- and folate-directed mutants. These modest changes attest to the resiliency of this enzyme and the chemical step. Even replacement of Asp-27 yields a mutant protein still capable of hydride delivery at low pH when solvent can protonate the ring (Howell et al., 1986). In contrast, removal of Ser-221 (S221A) in the catalytic triad of subtilisin causes a more convincing attrition in catalysis (Wells et al., 1986; Bryan et al., 1986). This mutation lowers k_{cat} by a factor of 2×10^6.

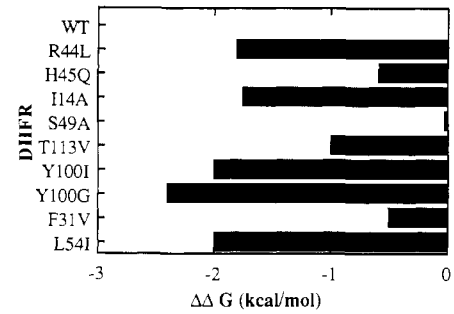

FIGURE 4: The difference in free energies (in kilocalories per mole) for hydride transfer for a number of folate- and coenzyme-directed mutants relative to wild type. $\Delta\Delta G = \Delta G$(wild type) – ΔG(mutant). Data for L54I were taken from Murphy and Benkovic (1989); data for T113V were taken from Fierke and Benkovic (1989); data for F31V were taken from Chen et al. (1987); data for R44L and H45Q were taken from Adams et al. (1989).

The equivalent effects of Y100I, Y100G, S49A, and I14A compared to a diverse battery of site-specific mutants (Figure 4) that involve hydrogen bonding, hydrophobic, and electrostatic disruptions at both binding sites do not support unique transition-state stabilization mechanisms directed toward the nicotinamide in the transition state. The proposal (Bystroff et al., 1990) that the hydroxyl of Tyr-100 may contort the reduced nicotinamide ring in the ground state so that it may adopt a structure closer to that of the transition state and thus be a principal source of DHFR's catalytic power is in disagreement with two particular experimental findings: (1) removal of Tyr-100 does not relieve the strain and lead to tighter binding of NADPH to Y100I and Y100G, and (2) the rates of hydride transfer are no more affected by replacements at position 100 than they are affected by substitutions away from the nicotinamide ring.

The free energy barrier leading to DHFR's transition state is certainly a function of the donor–acceptor distance and hydride trajectory. Using the dihydropyridine–methyleniminium cation reaction as a theoretical model, Wu and Houk (1987) have defined a transition state that incorporates the syn orientation of the reactants, a slightly boatlike structure for the pyridinyl ring and a nonlinear hydride transfer. Furthermore, these authors have evaluated the optimal C–C bond distance to be 2.6 Å. This is supported by the transition-state model building of Bystroff et al. (1990) from the ternary E–$NADP^+$–fol complex of *E. coli* DHFR. The former authors have also postulated that elongation of the optimal C–C bond distance by 0.1 or 0.3 Å leads to an increase in the hydride transfer activation energy of 0.7 and 5 kcal/mol, respectively. In the likelihood that point mutations in DHFR cause perturbations in this optimal distance equal to or exceeding 0.1 or 0.3 Å, the 2 kcal/mol window for observed changes in activation energy (Figure 4) suggests a broad potential energy surface for the enzyme or the occurrence of multiple substrate conformations only one pair of which is poised for hydride transfer.

These and other studies of single-site mutants of DHFR have shown that the replacements of active-site residues have predictable effects on hydride transfer. Also, in many cases, these mutations are not conservative yet still have the same effects as the conservative replacements. For instance, mutations of Phe-31 to Tyr or Gly lower hydride transfer equally although the two side chains differ largely in volume (Chen et al., 1987). In addition, replacements of Tyr-100 with Ile or Gly have the same effects on rate (Figure 4). However, since the energy barrier for hydride transfer is 2.6 kcal/mol lower than the product dissociation step (950 vs 12 s^{-1}), what is the selective advantage of possessing a conserved active-site residue that upon mutation is no less efficient in converting substrate to product? For some mutations the answer is simple; replacement of the conserved residue causes deleterious effects on other aspects of the catalytic mechanism. The high efficiency of DHFR is achieved through a low diffusional barrier for the substrate on the enzyme, rapid desorption of product, and a fast chemical step (Fierke et al., 1987). For instance, although R44L reduces the rate of hydride to a value still above the wild-type k_{cat}, the decreased affinity of NADPH for the ternary complex, E-NADPH-H_4F, allows slower observed dissociation of H_4F from the binary complex under physiological conditions of 1 mM NADPH. Thus, R44L is less efficient than wild-type DHFR. Likewise, substitution of Leu-54 with Gly has a similar effect on hydride, yet the binding of H_2F is reduced so that V/K is lowered from 24 to 0.1 μM^{-1} s^{-1} for this mutant (Mayer et al., 1986).

In the case of the mutants discussed in this paper, the evolutionary advantage of the conservation of S49 is not apparent from a kinetic perspective, while the catalytic efficiency under cellular conditions is decreased for either Y100 or I14 substitutions due to coupling a modest decrease in k_{cat}/K_M with increased product ($NADP^+$) inhibition or decreased activity at physiological pH, respectively.

ACKNOWLEDGMENTS

We thank Dr. Kenneth A. Johnson for the use of the stopped-flow apparatus and Kaye Yarnell for the typing of the manuscript.

Registry No. NADPH, 53-57-6; Tyr, 60-18-4; Ser, 56-45-1; Ile, 73-32-5; DHFR, 9002-03-3; deuterium, 7782-39-0.

REFERENCES

Adams, J., Johnson, K., Matthews, R., & Benkovic, S. J. (1989) *Biochemistry 28*, 6611–6618.

Appleman, J. R., Howell, E. E., Kraut, J., & Blakley, R. L. (1988) *J. Biol. Chem. 265*, 5579–5584.

Baccanari, D., Phillips, A., Smith, S., Sinski, D., & Burchall, J. (1975) *Biochemistry 14*, 5267.

Barshop, B. A., Wren, R. F., & Frieden, C. (1983) *Anal. Biochem. 130*, 134–145.

Benkovic, S. J., Fierke, C. A., & Naylor, A. (1988) *Science 239*, 1105–1110.

Birdsall, B., Burgen, A. S. V., & Roberts, G. C. K. (1980) *Biochemistry 19*, 3723–3731.

Birktoft, J. T., & Banaszak, L. J. (1984) in *Peptide and Protein Reviews* (Hearn, M. T. W., Ed.) Vol. 4, pp 1–46, Marcel Decker Inc., New York.

Blakley, R. L. (1960) *Nature (London) 188*, 231–232.

Bryan, P. N., Rollenca, M.-L., Pantoliano, M. W., Wood, J., Finzel, B. C., Gilliland, G. L., Howard, A. J., & Poulos, T. L. (1987) *Proteins: Struct., Funct., Genet. 1*, 326–334.

Burley, S. K., & Petsko, G. A. (1986) *FEBS Lett. 203*, 139–143.

Bystroff, C., Oatley, S. J., & Kraut, J. (1990) *Biochemistry 29*, 3263–3277.

Cayley, P. J., Dunn, S. M. J., & King, R. W. (1981) *Biochemistry 20*, 874–879.

Chen, J.-T., Taira, K., Tu, C.-P., & Benkovic, S. J. (1987) *Biochemistry 20*, 4093–4100.

Cook, P. F., Oppenheimer, N. J., & Cleland, W. W. (1981) *Biochemistry 20*, 1817–1825.

Curthoys, H. P., Scott, J. M., & Rabinowitz, J. C. (1972) *J. Biol. Chem. 247*, 1959–1964.

Dawson, R. M. C., Elliot, D. C., Elliot, W. H., & Jones, K. M. (1969) in *Data for Biochemical Research*, Oxford University Press, Oxford, England.

Dunn, S. M. J., & King, R. W. (1980) *Biochemistry 19*, 766–773.

Dunn, S. M. J., Bathcelor, J. G., & King, R. W. (1978) *Biochemistry 17*, 2356–2364.

Dyson, R. D., & Isenberg, I. (1971) *Biochemistry 10*, 3233–3241.

Fierke, C. A., Johnson, K. A., & Benkovic, S. J. (1987) *Biochemistry 26*, 4085–4092.

Filman, D. J., Bolin, J. T., Matthews, D. A., & Kraut, J. (1982) *J. Biol. Chem. 257*, 13663–13672.

Hanahan, D. (1983) *J. Biol. Chem. 166*, 557–580.

Howell, E. E., Villafranca, J. E., Warren, M. S., Oatley, S. J., & Kraut, J. (1986) *Science 231*, 1123–1128.

Johnson, K. A. (1986) *Methods Enzymol. 134*, 677–705.

Kallen, R. G., & Jencks, W. P. (1966) *J. Biol. Chem. 241*, 5845–5850.

Legerski, R. J., & Robberson, D. L. (1985) *J. Mol. Biol. 181*, 297–312.

Li, L., & Benkovic, S. J. (1991) *Biochemistry 30*, 1470–1478.

Maharaj, G., Selinsky, B. S., Appleman, J. R., Perlman, M., London, R. E., & Blakley, R. L. (1990) *Biochemistry 29*, 4554–4560.

Matthews, C. K., & Huennekens, F. M. (1960) *J. Biol. Chem. 235*, 3304–3308.

Matthews, D. A., Alden, R. A., Bolin, J. T., Freer, S. T., Hamlin, R., Xuong, N., Kraut, J., Poe, M., Williams, M., & Hoogsteen, K. (1977) *Science 197*, 452–455.

Mayer, R. J., Chen, J.-T., Taira, K., Fierke, C. A., & Benkovic, S. J. (1986) *Proc. Natl. Acad. Sci. U.S.A. 83*, 7718–7720.

Murphy, D. J., & Benkovic, S. J. (1989) *Biochemistry 28*, 3025–3031.

P-L Biochemicals (1961) Circular OR-18, P-L Biochemicals, Milwaukee, WI.

Poe, M., Greenfield, N. J., Hirshfield, J. M., & Hoogsteen, K. (1974) *Cancer Biochem. Biophys. 1*, 7.

Rabinowitz, J. C. (1960) in *Enzymes, 2nd Ed.* (Boyer, P. D., Lardy, H., & Myrbaeck, K., Eds.) Vol 2, pp 185–252, Academic Press, New York.

Sanger, F., Nicklen, S., & Coulson, A. R. (1977) *Proc. Natl. Acad. Sci. U.S.A. 74*, 5463.

Seeger, D. R., Cosulick, D. B., Smith, J. M., & Hulquist, M. E. (1949) *J. Am. Chem. Soc. 71*, 1753–1758.

Segel, I. H. (1975) in *Enzyme Kinetics, Behavior and Analysis of Rapid Equilibrium and Steady-State Enzyme Systems*, p 109, Wiley, New York.

Selinsky, B. S., Perlman, M. E., London, R. E., Unkefer, C. J., Mitchell, J., & Blakley, R. L. (1990) *Biochemistry 29*, 1290–1296.

Smith, D. R. (1985) *Annu. Rev. Genet. 19*, 423–462.

Smith, D. R., & Calvo, J. M. (1980) *Nucleic Acids Res. 8*, 2255–2274.
Stone, S. R., & Morrison, J. F. (1982) *Biochemistry 21*, 3757–3765.
Stone, S. R., & Morrison, J. F. (1984) *Biochemistry 23*, 2753–2758.
Stryer, L., & Haugland, R. P. (1967) *Proc. Natl. Acad. Sci. U.S.A. 58*, 719–726.
Taira, K., & Benkovic, S. J. (1988) *J. Med. Chem. 31*, 129–137.
Viola, R. E., Cooke, P. F., & Cleland, W. W. (1979) *J. Med. Chem. 96*, 334–340.
Wallace, R. B., Schold, M., Johnson, M. J., Dembeck, P., & Itakura, I. (1981) *Nucleic Acids 9*, 3647.
Wells, J. A., Powers, D. B., Bott, R. R., Graycar, T. P., & Estell, D. A. (1987) *Proc. Natl. Acad. Sci. U.S.A. 84*, 1219–1223.
Winberg, G., & Hammarskjold, M.-L. (1980) *Nucleic Acids Res. 8*, 253–264.
Wu, Y. D., & Houk, K. N. (1987) *J. Am. Chem. Soc. 109*, 2226.
Zoller, M. J., & Smith, M. (1982) *Methods Enzymol. 154*, 329–350.

Functional Consequences of Engineering the Hydrophobic Pocket of Carbonic Anhydrase II†

Carol A. Fierke,* Tiffany L. Calderone, and Joseph F. Krebs
Department of Biochemistry, Duke University Medical Center, Durham, North Carolina 27710
Received May 31, 1991; Revised Manuscript Received August 26, 1991

ABSTRACT: Twelve amino acid substitutions of varying size and hydrophobicity were constructed at Val 143 in human carbonic anhydrase II (including Gly, Ser, Cys, Asn, Asp, Leu, Ile, His, Phe and Tyr) to examine the catalytic roles of the hydrophobic pocket in the active site of this enzyme. The CO_2 hydrase and *p*-nitrophenyl acetate (PNPA) esterase activities, the pK_a of the zinc–water ligand, the inhibition constant for cyanate (K_{OCN}), and the binding constants for sulfonamide inhibitors were measured for various mutants and correlated with the size and hydrophobicity of the substituted amino acid. The k_{cat}/K_M for PNPA hydrolysis and K_{OCN} are linearly dependent on the hydrophobicity of the amino acid at position 143. All of the activities of CAII are decreased by more than a factor of 10^3 when large amino acids (Phe and Tyr) are substituted for Val 143, but the CO_2 hydrase activity is the most sensitive to the size and structure of the substituted amino acid. Addition of a single methyl group (V143I) decreases the activity 8-fold, while substitution of valine by tyrosine essentially destroys the enzyme function (k_{cat}/K_M for CO_2 hydration is decreased by more than 10^5-fold). K_{OCN} does not increase until Phe is substituted for Val 143, suggesting that the cyanate and CO_2 binding sites are not identical. The functional data in conjunction with X-ray crystallographic studies of four of the mutants [Alexander et al., 1991 (following paper in this issue)] allow interpretation of the mutants at a molecular level and mapping of the region of the active site important for CO_2 association. The hydrophobic pocket, including residues Val 121 and Val 143, is important for CO_2 and PNPA association; if the pocket is blocked, substrates cannot approach the zinc–hydroxide with the correct orientation to react. The interaction between Val 143 and CO_2 is relatively weak ($\leq$0.5 kcal/mol) and nonspecific; the association site does not tightly hold CO_2 in one fixed orientation for reaction with the zinc–hydroxide. This mechanism of catalysis may reflect a decreased requirement for specific orientation by CO_2 since it is a symmetrical molecule.

Carbonic anhydrase is a small, monomeric zinc metalloenzyme which catalyzes the reversible hydration of carbon dioxide to bicarbonate and a proton [recent reviews: Coleman (1986), Lindskog (1986), Silverman and Lindskog (1988), and Christianson (1991)]. This enzyme is ubiquitous in living systems, playing a large role in animal and plant metabolism including CO_2 transport, secretory processes, and photosynthesis. Carbonic anhydrase II (CAII)[1] is an extremely efficient catalyst; the second-order rate constant approaches the diffusion-controlled limit ($k_{cat}/K_M^{CO_2} = 1.5 \times 10^8$ M^{-1} s^{-1}) and its turnover number ($k_{cat}^{CO_2} = 1.4 \times 10^6$ s^{-1}) is one of the highest measured. In addition to its CO_2 hydrase activity, CAII will catalyze hydrolysis of many aromatic esters (Pocker & Sarkanen, 1978) and is potently inhibited by aromatic sulfonamides (King & Burgen, 1976).

The three-dimensional structure of human erythrocyte CAII has been solved by X-ray crystallography to 2.0-Å resolution (Liljas et al., 1972) and further refined (Eriksson et al., 1986, 1988a) revealing that the zinc cofactor is located near the center of the enzyme close to the bottom of a 15-Å-deep

†Supported by grants from the National Institutes of Health (GM40602) and the American Cancer Society (JFRA-246) and a Fellowship in Science and Engineering from the David and Lucile Packard Foundation.
*Corresponding author.

[1] Abbreviations: CAII, human carbonic anhydrase II; PNPA, *p*-nitrophenyl acetate; MES, 2-(*N*-morpholino)ethanesulfonic acid; OCN, cyanate; MOPS, 4-morpholinepropanesulfonic acid; TAPS, [tris(hydroxymethyl)methyl]aminopropanesulfonic acid; EDTA, (ethylenedinitrilo)tetraacetic acid; DNSA, dansylamide; ACET, acetazolamide; wt, wild-type; V143G, Val 143 → Gly; V143C, Val 143 → Cys; V143L, Val 143 → Leu; V143I, Val 143 → Ile; V143N, Val 143 → Asn; V143S, Val 143 → Ser; V143H, Val 143 → His; V143F, Val 143 → Phe; V143Y, Val 143 → Tyr; V143D, Val 143 → Asp.

0006-2960/91/0430-11054$02.50/0 © 1991 American Chemical Society